Author Manuscript

Title: Ag-Au-bimetal incorporated ZnO-nanorods photo-anodes for efficient photo-electrochemical splitting of water

Authors: Sandesh R. Jadkar, Prof. Dr.; Vidhika Sharma; Mohit Prasad; Avinash Rokade; Perumal Ilaiyaraja; Chandran Sudhakar

To be cited as: 10.1002/ente.201800581

Link to VoR: https://doi.org/10.1002/ente.201800581

Ag-Au-bimetal incorporated ZnO-nanorods photo-anodes for efficient photoelectrochemical splitting of water

Vidhika Sharma,[a] Mohit Prasad*,[a] Avinash Rokade,[a] Perumal Ilaiyaraja,[b] Chandran Sudakar,[b] and Sandesh Jadkar*[a]

Abstract: Plasmonic Ag-Au/ZnO nanorods (ZNRs) based photo-anodes were synthesized using a simple electrochemical route and were then evaluated for photoelectrochemical (PEC) activity. The amalgamation of Ag and Au nanoclusters broadens the UV-Vis light absorption in the range of 400 nm to 650 nm. Ag-Au/ZNRs photo-anodes had shown photocurrent density of ~1.4 mA cm^{-2}, at a bias of 0.75 V/SCE, which is ~3.1 times of bare ZNRs photo-anode. Bi-metallic Ag-Au/ZNRs based photo-anode shows the maximum photo-conversion efficiency of 0.77% at 0.5 V/SCE, under one sun illumination. Formation of hot electrons in Ag-Au/ZNRs photo-anodes can be partly held responsible for the enhanced PEC activity. Au/Ag core/shell morphology evolves when a thin layer of Ag is loaded on Au nanoparticles. For an in-depth analysis on Ag-Au incorporated ZNRs based photo-anodes and its PEC activity, a detailed characterization was carried out using physico-chemical, spectral and microscopy techniques. The analysis shows that Au in direct contact with ZnO interacts mainly with oxygen vacancies present on surface of ZnO and Ag interacts with Au for an effective electron-hole segregation process at their interface and electron storage occurs in metal nanoparticles. The results suggest bi-metal incorporated ZNRs based photo-anodes can be a prospective candidate for PEC water splitting application.

Introduction

Global energy problem can be solved by one of the most sustainable and attractive solution which is solar to chemical energy route [1]. In spite of several efforts made by numerous researchers, we are still far away from any remarkable solution that can make this technology a household proposition. PEC splitting of water is the most viable solar to chemical route which is still impeded by the development and realization of an ideal semiconductor photo-anode. A major snag in photo-anodes is low light activity. Noble-metal nano-clusters loaded on semiconductors can enhance the visible light absorption through surface plasmon resonance (SPR) [2]. Numerous research studies have been reported which utilizes SPR phenomenon for enhancing visible light absorption in photo-anodes but there are very few reports on the use of bi-metallic nanoparticles in PEC splitting of water [3]. Bi-metallic nanoparticles in which two different types of metal present in conjunction with each other, are distinct and exhibit salient features than mono-metals [4]. Bi-metal nanoparticles incorporated photoanodes exhibits very unique and remarkable properties (electrical and optical) and can have applications in PEC regime. Thus the PEC activity of ZnO on any other semiconductor can be enhanced by loading them with these bi-metallic nanoparticles such as Ag-Au, Au-Pt, or Ag-Pt etc. Ag and Au both exhibit SPR phenomenon in different wavelength regimes in visible light.

ZnO is one of the most attractive material for PEC splitting of water but its inherent broad band gap of 3.2 eV limits its full potential for PEC activity [5]. To overcome the above limitation exhibited by ZnO there is a requirement of solar light absorption in the visible range along with electronic integration of light absorbing redox site components. This is possible by integrating plasmonic metal nanostructures exhibiting SPR which provide charge carriers to the ZnO. Fermi level tuning can be controlled using dopants, filters, co-catalyst and different other methods [6]. Metals exhibit collective oscillation of electrons induced by visible light absorption which depends on the shape, size and dielectric constant of the surrounding medium. These metals interact at different frequency of solar light and produce local electromagnetic field [7]. Syntheses of bi-metal incorporated nanostructures provide an alternative pathway for enhancing the SPR wavelength regime. Many research studies have focused on bi-metallic nanoparticles, but Ag and Au together has an advantage of similar lattice constants [4(a)]. This allows Ag-Au to formulate different types of nanostructure/nano-composites. Bi-metal systems comprising of Ag-Au act as a plasmonic antenna. The SPR absorptions of Ag and Au nanoparticles individually occur at 420 and 550 nm respectively, however the concurrent absorption phenomena occurring in complementary wavelength regime of the solar spectrum is not fully utilized [8]. The integration of Ag-Au bi-metallic nanoparticles with ZnO is crucial for PEC applications. The current density enhances after incorporation of bi-metallic systems which is clearly evident from the photocurrent measurements.

In the current study we have electrodeposited bi-metallic Ag-Au nanoparticles on ZnO nanorods and demonstrated the enhanced PEC activity of the synthesized photo-anodes. The electronic integration of metal nanoparticles with ZNRs and the formation of hetero-junctions is the key aspect for achieving enhanced PEC activity. The present research paper demonstrates a very simple process to synthesize bi-metallic nanoparticles incorporated ZNRs based photo-anodes where bi-metals play multiple roles; (i) bi-metals Ag-Au acts as sensitizer in ZNRs based photo-anodes and enhances light absorption due to localized surface plasmons, (ii) interaction of localized electric field of bi-metals with ZNRs generates electron hole pair near the nanorods surface and easily separate them due to surface barrier, and (iii) surface capping by thin metallic layer reduces trap site and minimizes the trapping of holes [9]. We have synthesized Au-ZNRs photo-anodes with Au loaded on ZNRs photo-anodes for 60, 300 and 600 s respectively. Among these

[a] Mohit Prasad, Sandesh Jadkar
Department of Physics
Savitribai Phule Pune University
Ganesh Khind Road, Pune 411 007 (India)
E-mail: mohitprasad7@gmail.com, sandesh@physics.unipune.ac.in
[b] Multifunctional Materials Laboratory
Department of Physics, Indian Institute of Technology Madras, Chennai-600 036 (India)
Supporting information for this article is given via a link at the end of the document.((Please delete this text if not appropriate))

photo-anodes Au-ZNRs-300 exhibited the best PEC response and hence it was chosen for further loading of plasmonic Ag nanoparticles, and is denoted as Ag-Au-ZNRs in the whole manuscript. All the synthesized photo-anodes were characterized using different techniques XRD, UV-Vis, Impedance, and Mott Schottky. PEC, Applied bias photon to current efficiency (ABPE) and Incident photon to current efficiency (IPCE) measurements were carried out to understand the intricate nature of photo-anodes for PEC water splitting application.

Results and Discussion

Figure 1 shows the diffraction patterns of all the synthesized samples i.e. Au-ZNRs and Ag-Au-ZNRs indexed to the hexagonal wurtzite structure of ZnO. A very sharp and intense peak occur at 2θ = 34.2°, is assigned to ZnO (002) planes of hexagonal wurtzite phase of ZNRs. Loading of Au results in appearance of an additional peak in XRD spectrum at 38.1°, which is Au (111) diffraction peak. Au and Ag have their overlapping diffraction peaks appearing at 38.1°(111) plane as they have closely matched spaced lattices [10]. All these synthesized photo-anodes have diffraction peaks corresponding to ZnO and Ag-Au. The presence of Ag and Au on ZNRs is further confirmed by EDX analysis and elemental mapping for both the plasmonic metals has been recorded.

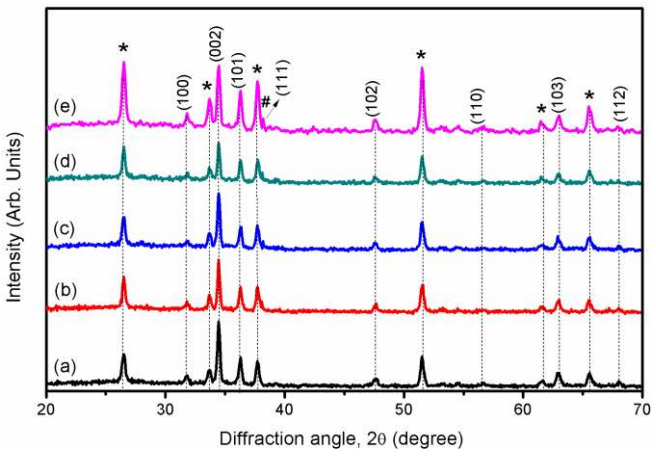

Figure 01: XRD spectra of **a)** Bare ZNRs **b)** Au- ZNRs -60s **c)** Au-ZNRs-300s **d)** Au-ZNRs-600s **e)** Ag-Au-ZNRs photo-anodes (* indicates FTO peaks, # indicates Au and Ag).

The surface morphology of all the synthesized photo-anodes was carried out using FESEM. Figure 2 shows the FESEM images of bare ZNRs, Au-ZNRs and Ag-Au-ZNRs based photo-anodes. The diameter of all the nanorods samples were distributed in the range of ~ 50-60 nm. The length of the ZNRs was ~ 1 µm, which corresponds to an aspect ratio of 200 nm. FESEM images reveal that Au and Ag nanoparticles are uniformly dispersed and have properly attached on the surface of nanorods. The dispersion of both the plasmonic nanoparticles doesn't disturb the morphology of the ZnO nanostructure and appears to be attached and distribute evenly on the exterior surface of ZNRs. The particle size of the electrodeposited Au and Ag nanoparticles was estimated using Image J software and was found to be in the range of ~12-30 nm. EDX analysis was carried out to study the atomic % of all the atoms in the synthesized photo-anodes. The elemental mapping of individual elements from a selected area of synthesized photo-anodes is illustrated in Figs. S1, S2 and the mapping is in agreement with the structure of desired photo-anodes. The electrodeposition process reported in this manuscript offers an easily executed and in-situ process for plasmonic modified hierarchical 1D nanostructure of ZnO.

Figure 3 shows the UV-Vis absorption spectra of all the synthesized photo-anodes. Au nanoparticles have SPR phenomena active in the range of 500 and 650 nm. The loading of Ag over Au-ZNRs, results in a broad peak that was observed in the lower wavelength region. The Ag-Au-ZNRs becomes more active in the visible light absorption region between 400-650 nm [4a]. The Ag deposition over Au-Z-NRs is solely responsible for the broadening of the localized SPR and it also increases the imaginary component of dielectric function of metals. The loading of Ag over Au-ZNRs results in the formation of hot electrons due to fast rate of localized SPR relaxation. A detailed comparison of the bare ZNRs, Au-ZNRs and Ag-Au-ZNRs spectra reveals that all the photo-anodes absorb at 400 nm, but in Ag-Au-ZNRs photo-anodes, the absorption takes place even below 400 nm. The spectrum further confirms that a significant UV absorption takes place when Ag is incorporated and this is also confirmed by the rise in the absorption coefficient at 400 nm. The incorporation of bi-metals extends the light absorption between 400 and 650 and an elevated light absorption in Ag-Au-ZNRs reflects the predominance of Ag over Au. Thus, incorporation of bi-metals on ZNRs photo-anodes helps in extending absorption range over the visible region.

Due to the enhanced visible absorption caused by SPR, Ag and Au plasmonic nanoparticles prolong the life time of photo-generated charge carriers. Electrochemical impedance spectroscopy (EIS) was performed using 0.5 M Na_2SO_4 electrolyte and with an applied bias of 0.5 V. The frequency was swept in the range of 0.1 to 100 kHz. Ag-Au-ZNRs and Au-ZNRs photo-anodes exhibited one single arc which suggests that surface charge transfer is the only process involved in the PEC reaction. In EIS Nyquist plot, arc diameter is inversely proportional to the fast rate of interfacial charge transfer process and effective charge separation of photo-generated charge carriers. Moreover, the arc diameter of Ag-Au-ZNRs clearly indicates a likely larger lifetime of charge carrier in the synthesized photo-anodes as shown in figure 4.

Mott-Schottky (MS) measurements of all the synthesized photo-anodes were performed under dark at a frequency of 500 Hz to obtain the flat band potential and donor density [11]. The loading of Ag and Au and their effect on the electronic properties of synthesized photo-anodes can be evaluated using this technique. A more negative value of flat band potential compared to bare-ZNRs indicates that more field is available for charge carrier to segregate at the same potential. From the

thermodynamic perspective a negative shift in flat band potential indicate 1) reduction in free energy for transfer of charge carrier and 2) an increase in free energy change for charge recombination. All the photo-anodes exhibited positive slope as visible from MS plot shown in figure 5 indicating their n-type character. Ag-Au-ZNRs demonstrated a remarkably smaller slope in the MS plot than bare and Au-ZNRs, which clearly suggest an increase in donor density due to bi-metallic loading.

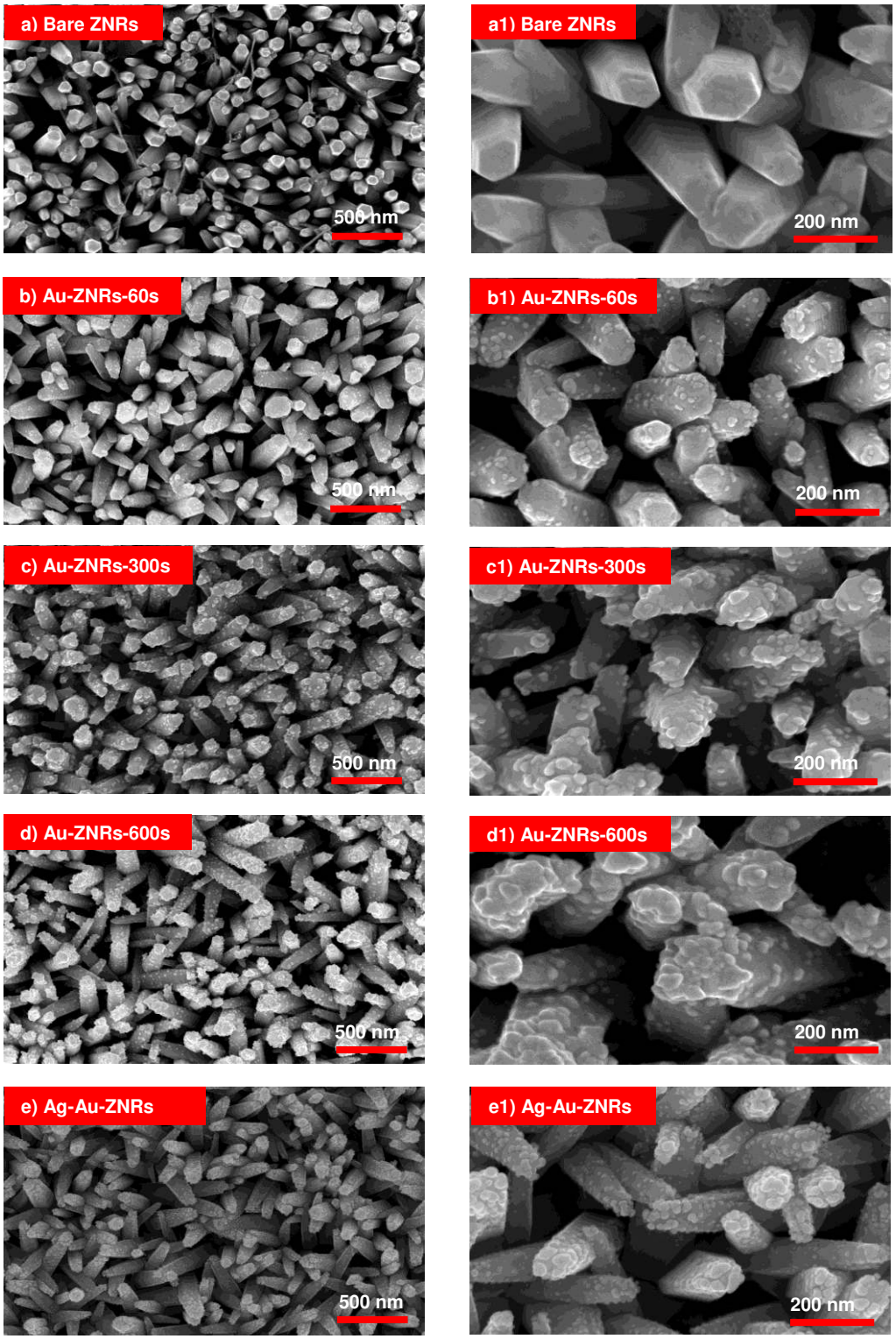

Figure 02a: FE-SEM micrographs of a) Bare ZNRs b) Au-ZNRs-60s c) Au-ZNRs-300s d) Au-ZNRs-600s e) Ag-Au-ZNRs at low magnification (LM) and FE-SEM micrographs of a) Bare ZNRs b) Au-ZNRs-60s c) Au-ZNRs-300s d) Au-ZNRs-600s e) Ag-Au-ZNRs at high magnification (HM).

The carrier density of all the photo-anodes was calculated from the slope of MS plot [11]. The calculated electron densities of bare ZNRs, Au-ZNRs-60, Au-ZNRs-300, Au-ZNRs-600 and Ag-Au-ZNRs are $1.7x10^{18}$, $5.5x10^{18}$, $2.4x10^{19}$, $1.0x10^{19}$, and $3.5x10^{19}$ cm^{-3}, respectively.

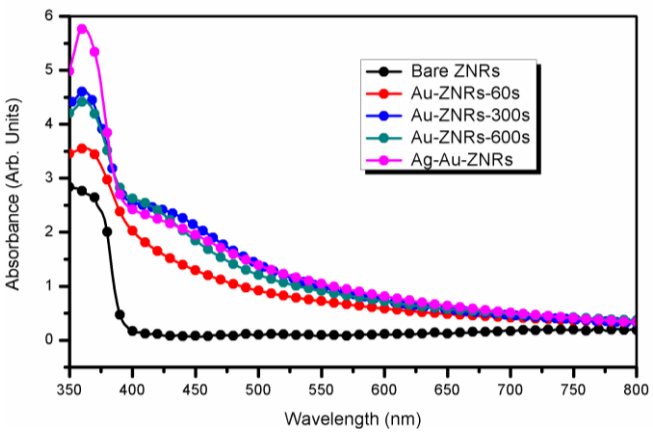

Figure 03: UV-Visible absorption spectra of bare ZNRs, Au-ZNRs-60s, Au-ZNRs-300s, Au-ZNRs-600s and Ag-Au-ZNRs photo-anodes.

There is ~20 times increase in the carrier density of Ag-Au-ZNRs (compared to bare ZNRs) which is evident from the comparison of the slopes of MS plot of all the synthesized photo-anodes. Increase in electron density of Ag-Au-ZNRs is due to loading of plasmonic bi-metals Ag and Au over ZNRs. This increase favors charge transport and thus directly contributes to PEC reaction.

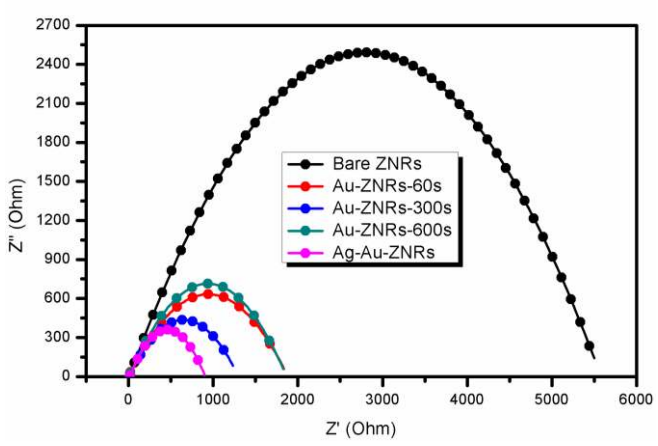

Figure 04: Nyquist plots of photoelectrochemical impedance spectra of bare ZNRs, Au-ZNRs-60s, Au-ZNRs-300s, Au-ZNRs-600s and Ag-Au-ZNRs photo-anodes s at 0.5 V under illumination in 0.5 M Na_2SO_4.

The depletion layer width of ZNRs, Au-ZNRs-60, Au-ZNRs-300, Au-ZNRs-600 and Ag-Au-ZNRs based photo-anodes are 29.5, 16.0, 7.8, 12.3 and 6.6 nm respectively. Normally, formation of a thin depletion layer enables easier diffusion of photo-generated charge carriers which in turn is a favorable characteristic of PEC activity.

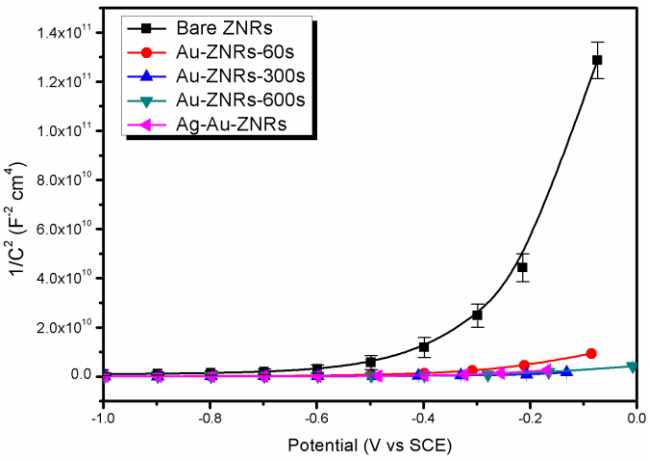

Figure 05: Mott-Schottky plots for bare ZNRs, Au-ZNRs-60s, Au-ZNRs-300s, Au-ZNRs-600s and Ag-Au-ZNRs photo-anodes.

Open circuit potential (OCP), i.e. the potential generated at the working electrode (WE) with respect to the reference electrode (RE) when no current is drawn from WE. The OCP measurements can be used to understand the intricate nature of all the synthesized photo-anodes [12]. OCP is measured as a function of time under light ON and OFF conditions and the same are plotted for all the synthesized photo-anodes in figure 6.

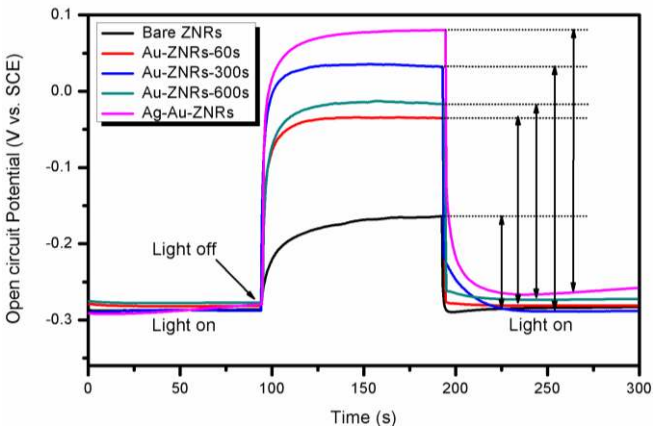

Figure 06: Open Circuit Potential measurements for bare ZNRs, Au-ZNRs-60s, Au-ZNRs-300s, Au-ZNRs-600s and Ag-Au-ZNRs photo-anodes under light ON and OFF conditions.

In open circuit condition, under illumination electrons accumulate within the film and shift the Fermi level to negative potential thereby resulting in a cathodic shift of OCP. This cathodic shift is the prime characteristic of material with n-type nature [12b]. The maximum photo potential (i.e. Voc $_{Light}$ – Voc $_{Dark}$) has been observed for Ag-Au-ZNRs based photo-anode among all the

synthesized photo-anodes. A large photopotential leads to more cathodic potential thereby reducing H_2O into H_2. For all the synthesized photo-anodes, under illumination the value of OCP reaches the steady state value on attaining initial maxima but diminishes gradually after switching off the light at different rates in all the samples. The recombination of carriers is solely responsible for the reduction in the value of OCP as soon as light is turned off. The rate of recombination directly governs the decay rate of OCP. The slower decay rate of OCP exhibited by Ag-Au-ZNRs compared to other films indicate small rate of recombination and therefore enhanced lifetime of charge carriers. The following equation has been used to calculate the carriers' lifetime [13].

$$\tau = -kT/q\ (dVoc/dt)^{-1} \quad (1)$$

Where k is Boltzmann constant, T is the temperature in Kelvin and q is the elementary charge. The lifetime of the charge carriers in ZNRs, Au-ZNRs-60s, Au-ZNRs-300s, Au-ZNRs-600s and Ag-Au-ZNRs is 31, 63, 82, 67 and 93 ms respectively. Thus it can be deduced that the loading of Ag and Au over ZNRs based photo-anodes suppress recombination and increases the lifetime of photo-generated charge carriers.

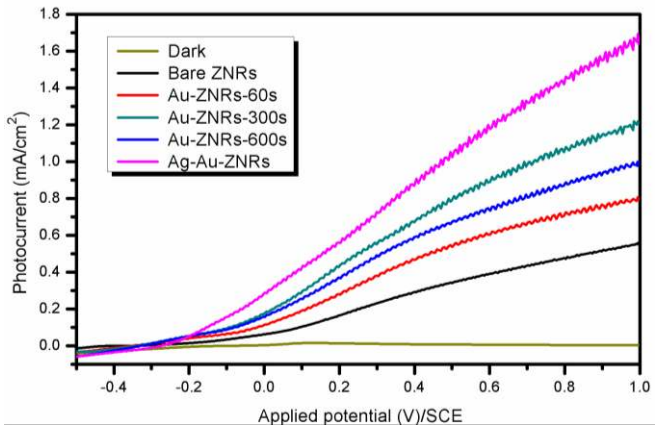

Figure 07: Photocurrent curves recorded for bare ZNRs, Au- ZNRs-60s, Au-ZNRs-300s, Au-ZNRs-600s and Ag-Au-ZNRs photo-anodes with a scan rate of 20 mV/s in the applied potential from -1.0 to 1.0 V (vs. SCE) under AM 1.5 simulated solar light

A three electrode system with SCE as reference, and Pt as counter electrode was used to study the PEC properties of all the synthesized photo-anodes. Figure 7 shows the linear sweep voltammetry recorded in 0.5 M Na_2SO_4 electrolyte solution under 1 Sun illumination (with an intensity of 100 mW/cm^2). The loading of Au over ZNRs helps in increasing the photocurrent density. Further loading of Ag over Au-ZNRs based photo-anode leads to a significant increase in the photocurrent density of ZNRs based photo-anodes. The photocurrent density of Ag-Au-ZNRs is almost ~1.4 times (at 0.75 V vs SCE) that of Au-ZNRs-300s based photo-anodes which clearly highlights the effective light harvesting by Ag and Au composite. The graph in figure 7 shows the positive role of Ag in enhancing the photoresponse of Au-ZNRs based photo-anodes. Basically, the role of plasmonic nanoparticles is to transfer charge to the semiconductor which eventually results in an enhanced photocurrent. The loading of Ag plasmonic nanoparticles over Au-ZNRs photo-anode increases the electron density around the Au nanoparticles and the SPR-excited form of bi-metals enhances the electron transfer from bi-metallic plasmonic nanoparticles to the semiconductor. Plasmonics assisted enhancement in PEC splitting of water can be explained with two possible mechanisms available in the literature i.e Resonance energy transfer (RET) and direct energy transfer (DET). RET takes place when both metal and semiconductor are not in direct contact with each other, whereas DET takes place when both the plasmonic metal and the semiconductor are in direct contact with each other [14]. In the present study the second mechanism is the most relevant. Upon visible light absorption, the bi-metallic nanostructure excites to its surface plasmon state, DET transfer electrons from the surface plasmon state to the ZnO conduction band. This is facilitated by the band energy alignments, i.e. the energy of ZnO is lower than metal SPR state. Overall loading of Ag over Au-ZNRs enhances the electron transfer process.

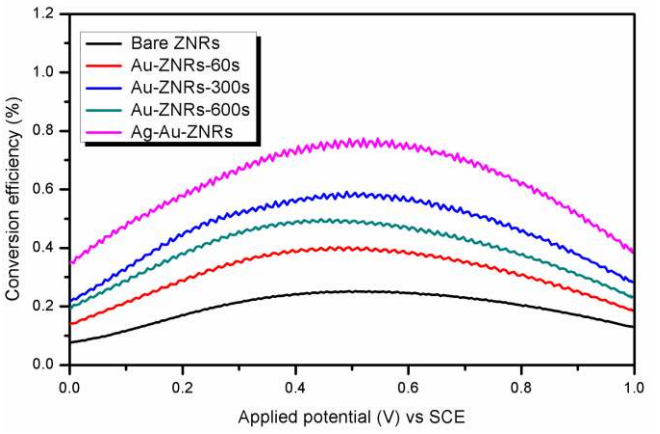

Figure 08: ABPE curves recorded bare ZNRs, Au-ZNRs-60s, Au-ZNRs-300s, Au- ZNRs-600s and Ag-Au-ZNRs photo-anodes

ZNRs immobilized with bi-metallic nanoparticles when excited with the absorption wavelength of bi-metals, electron hole pairs will be generated on the ZNRs surface. The migration of photogenerated electrons takes place from the valence band to the conduction band leaving the same number of holes in the valence band of the semiconductor. The presence of Au over ZNRs acts as core which facilitates the continuous migration of electron from the conduction band of ZNRs to the Au core. The conduction band edge of ZnO is -0.5 eV vs. NHE and the Fermi level of Au +0.5 eV vs. NHE, which causes smooth flow of electron from conduction band of ZNRs to Au core [15]. The loading of Ag over Au-ZNRs acts as shell layer and both the metallic nanoparticles (i.e. Au and Ag) interact with ZNRs. At the interface of Ag shell and ZNRs a new stable Fermi level is created. The work-function of ZnO is (~5.2 eV) higher than that of Ag (4.2 eV) and Au (5.1 eV), thus electrons migrate from metal nanoparticle to ZNRs [15b]. The Fermi level of Au-Ag-

ZNRs shifts up with respect to bare ZNRs and below with respect to Au-ZNRs. The electron hole pairs are generated in bi-metal embedded photo-anode as soon as the surface is excited with solar light. The work-function of Ag is positive related to Au, so it will enable the transfer of electron from the Ag shell to the Au core. In Ag-Au-ZNRs the charge separation is much better compared to Au-ZNRs which is directly responsible for enhanced PEC activity. In this manuscript, we have taken the best photo-anode of Au-ZNRs core-shell (with deposition time 300 s) and then loaded with plasmonic nanoparticle of Ag (with deposition time 100 s). The PEC results clearly indicate that loading of bi-metals helps in elevating the absorption range of ZNRs and thereby enhancing the PEC activity of the synthesized photo-anodes (see figure 8).

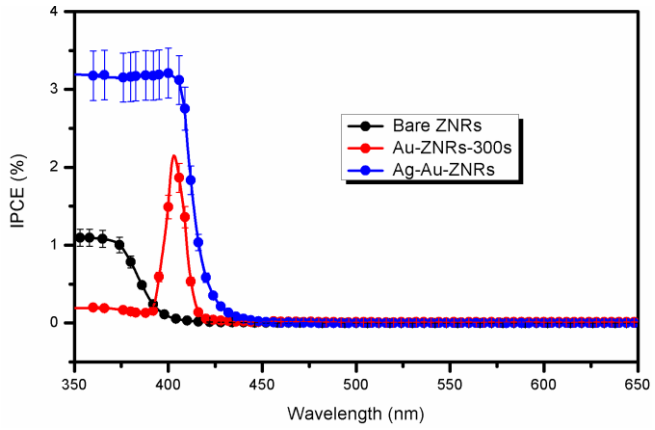

Figure 9: IPCE measurements of bare ZNRs, Au-ZNRs-300s and Ag-Au-ZNRs photo-anodes as a function of the wavelength

Incident photon to current efficiency (IPCE) was recorded to evaluate the efficiency of the system with respect to wavelength for the bare ZNRs and the best Au-ZNRs-300s and Ag-Au-ZNRs based photo-anodes as shown in Figure 9. IPCE is the measurement related to total number of photogenerated electrons per incident photon for a particular wavelength. A high IPCE value indicates improved generation and transportation of photogenerated charge carrier in ZNRs based photo-anodes when loaded with plasmonic bi-metals.

Conclusions

In this paper we have thoroughly investigated the role of bi-metal incorporation in ZNRs based photo-anodes for photoelectrochemical splitting of water. Loading of mono-metal on ZNRs (i.e. Au) enhances the PEC response of ZnO based photoanode, but when the same photoanode is loaded with bi-metals (i.e. Au and Ag) both of them work in conjunction and further enhances the PEC response. Ag-Au-ZNRs photo-anodes exhibited the photocurrent density of 1.4 mA cm^{-2} at a bias of 0.75 V/SCE, whereas optimized Au-ZNRs-300s photo-anode had shown photocurrent density of 1.0 mA cm^{-2} at same bias. The bi-metallic loading of plasmonic nanoparticles on ZNRs photo-anodes has been confirmed using various types of physical and chemical measurements. The results suggest that these photo-anodes can be efficiently used for water splitting application.

Experimental Section

A conventional three-electrode cell was used for electrochemical deposition. For synthesis of photo-anodes FTO was used as a conducting glass substrate. Saturated calomel electrode and Pt mesh act as reference and counter electrode. FTO substrates were cleaned using standard procedure prior to electrodeposition. ZNRs were synthesized in an aqueous solution comprising of 0.5 M $Zn(NO_3)_2.6H_2O$ and 50 mM $NaNO_3$ in an electrolyte bath having temperature of ~80 ºC. Step potentials of -1.3 and -1.0 V were applied for 15 and 2000 s respectively during electrodeposition [16]. The films were properly rinsed with de-ionized water and then dried at room temperature in air. To improve the crystallinity of ZnO nanorods thin films, the photo-anodes were sintered in air at 600 ºC. Au plasmonic nanoparticles were electrochemically deposited using solution of 0.0005 M $HAuCl_4.H_2O$ with applied potential of -0.24 V/SCE, for 60, 300 and 600 s. Further Ag plasmonic nanoparticles were electrochemically loaded on Au-ZNRs-300s photo-anode; using solution of 0.001 M $AgNO_3$ contained in 0.05 M Na_2SO_4 with applied potential of -0.40 V/SCE, for a time span of 100 s. After electrodeposition, all the fabricated thin films were dried at 100 ºC for 1 hr in oven.

XRD, UV-Vis spectroscopy was used to study the structural properties of the synthesized photo-anodes. XRD diffractometer (Bruker D8 Advance, Germany) was used to study the crystal structure of the synthesized photo-anodes using CuKα (λ = 1.54 Å) at a grazing angle of 1º. Jasco UV-670 was used to measure the absorption spectra of all the photo-anodes. FESEM, EDX and elemental mapping was performed using FEI, Nova NanoSEM 450 scanning electron microscope. EIS measurements were carried out using the Metrohm potentiostat (model: FRA 32 M). EIS measurements were recorded in 0.5 M Na_2SO_4 electrolyte at 0 V and the frequency was kept in the range of 0.1 to 100 kHz. The MS plot of all the synthesized photo-anodes ($1/C^2$ vs. electrode potential) was recorded under darkness at a frequency of 500 Hz to obtain flat band potential (V_{fb}) and donor density (N_d) [17]. Following equations were used to estimate the values of V_{fb} and N_d

$$\frac{1}{C^2} = \frac{2}{q\,\varepsilon_0\,\varepsilon_s\,N_D}\left[V - V_{fb} - \frac{(k_B T)}{q}\right] \quad (2)$$

$$S = \frac{2}{q\,\varepsilon_0\,\varepsilon_s\,N_D} \quad (3)$$

$$w = \left[\frac{2\varepsilon_s\varepsilon_0}{qN_D}(V - V_{fb})\right]^{1/2} \quad (4)$$

Where q is the electronic charge, ε_0 is permittivity of free space, ε_s is the dielectric constant of semiconductor electrode, k_B is Boltzman's constant, T is the temperature (in Kelvin), S is the slope of MS curve, and w is depletion layer width. The extrapolation of the linear portion of $1/C^2$ at x-axis is considered as the values of V_{fb}.

Metrohm Potentiostat (Model: PGSTAT101) was used for PEC measurement utilizing conventional three electrode system consisting of SCE and Pt as reference and counter electrode respectively with 0.5 M Na_2SO_4 electrolyte. The size of working electrode was ~1 cm^2 and sheet resistance of FTO ~7 Ω/sq. A solar simulator PECLO1 (100 mW/cm^2) was used for PEC measurements. The overall IPCE for bare ZNRs, Au-ZNRs-300s, and Ag-Au-ZNRs was investigated at various wavelengths in the spectral region (350-650 nm). The IPCE for all the synthesized photo-anodes was measured using an external quantum efficiency setup (Bentham PVE 300) under zero applied bias. In the two-electrode assembly, ZNRs, Au-ZNRs-300s and Ag-Au-ZNRs, coated FTO was used as the working electrode, Pt-coated FTO acted as the counter electrode, and 0.5 M aqueous Na_2SO_4 electrolyte was packed in between the two electrodes.

Acknowledgements

Mohit Prasad and Vidhika Sharma are thankful to University Grants Commission, Government of India for Dr. D. S. Kothari PostDoc Fellowship. Avinash Rokade is thankful to Ministry of New and Renewable Energy (MNRE), Government of India for National Renewable Energy (NRE) fellowship. Sandesh Jadkar is thankful to University Grants Commission, New Delhi for special financial support under UPE program.

Keywords: Electrodeposition • Bi-metal photo-anodes • Water splitting • PEC activity • Incident photon to current conversion efficiency (IPCE)

[1] D. Lips, J. M. Schuurmans, F. B. dos Santos, K. J. Hellingwerf, *Energy Environ. Sci.* **2018**, *11*, 10-22.

[2] K. H. Leong, A. A. Aziz, L. C. Sim, P. Saravanan, M. Jang, D. Bahnemann, *Beilstein J Nanotechnol.* **2018**, *9*, 628-648.

[3] a) K. K. Patra, C. S. Gopinath, *ChemCatChem* **2016**, *8*, 3294-3311; b) R. A. Rather, D. Pooja, P. Kumar, S. Singh, B. Pal, *J Clean Prod.* **2018.** *175*, 394-401; c) I. Majeed, U. Manzoor, F. K. Kanodarwala, M. A. Nadeem, E. Hussain, H. Ali, A. Badshah, J. A. Stride, M. A. Nadeem, *Catal. Sci. Technol.* **2018**, *8*, 1183-1193; d) P. Shahini, A. A. Ashkarran, *Colloids Surf. A Physicochem. Eng. Asp.* **2018**, *537*, 155-162; e) A. A. Melvin, K. Illath, T. Das, T. Raja, S. Bhattacharyya, C. S. Gopinath, *Nanoscale* **2015**, *7*, 13477-13488; f) N. Zhou, L. Polavarapu, N. Gao, Y. Pan, P. Yuan, Q. Wang, Q. H. Xu, *Nanoscale* **2013**, *5*, 4236-4241.

[4] a) L. M. Liz-Marzán, *Langmuir* **2006**, *22*, 32-41; b) L. M. Liz-Marzan, A. P. Philipse, *J Phys. Chem.***1995**, *99*, 15120-15128.

[5] a) T. Wang, R. Lv, P. Zhang, C. Li, J. Gong, *Nanoscale* **2015,** *7*, 77-81; b) P. Singh, N. Jadhav, *Int. J. Electroactive Mater.* **2015**, *3*, 1-5.

[6] a) S. B. A. Hamid, S. J. Teh, C. W. Lai, *Catalysts*, **2017**, 7, 93-107; b) M. Sahu, P. K. Singh, S. P. Pandey, B. Bhattacharya, *Macromol. Symp.* **2015**, *347*, 68-74.

[7] L. Zhou, T. Zhao, X. Y. Wang, L. D. Sun, C. H. Yan in *Bimetallic Nanostructures: Shape-Controlled Synthesis for Catalysis, Plasmonics, and Sensing Application*, *Vol.1* (Eds.: Y. W. Zhang), John Wiley & Sons. West Sussex **2018,** pp. 442-447.

[8] J. Zhu, *Nanoscale Res. Lett.* **2009**, *4*, 977-981.

[9] a) G. Liu, K. Du, J. Xu, G. Chen, M. Gu, C. Yang, K. Wang, H. Jakobsen, *J. Mater. Chem.* **2017**, *5*, 4233-4253; b) Q. Zhang, D. T. Gangadharan, Y. Liu, Z. Xu, M. Chaker, D. Ma, *J. Materiomics* **2017**, *3*, 33-50.

[10] Y Hashimoto, G Seniutinas, A Balčytis, S Juodkazis, Y Nishijima, *Scientific Reports* **2016,** *6*, 25010.

[11] a) Jr, C.F. Windisch, G.J. Exarhos, 2000. *J Vac Sci Technol A*, **2000**, *18*, 1677-1680; b) F. Fabregat-Santiago, G. Garcia-Belmonte, J. Bisquert, P. Bogdanoff, A. Zaban, *J. Electrochem. Soc.* **2003,***15*, E293-E298.

[12] a) Z. Chen, T. F. Jaramillo, T.G. Deutsch, A. Kleiman-Shwarsctein, A. J. Forman, N. Gaillard, R. Garland, K. Takanabe, C. Heske, M. Sunkara, E. W. McFarland, *J. Mater. Res.* 2010, *25*, 3-16; b) J. Liu, W. Luo, K. Zhu, X. Wen, F. Xiu, J. Yuan, Z. Zou, W. Huang, *RSC Adv.* **2017**, *7*, 30650-30656.

[13] A. Zaban, M. Greenshtein, J. Bisquert, *ChemPhysChem* **2003**, *4*, 859-864.

[14] J. Li, S. K. Cushing, P. Zheng, F. Meng, D. Chu, N. Wu, *Nat. Commun.* **2013**, *4*, 2651-2659.

[15] a) S. Chen, L.W. Wang, *Chem. Mater.* **2012**, *24*, 3659-3666. b) H. Li, H. Yu, X. Quan, S. Chen, Y. Zhang, *ACS Appl. Mater. Interfaces* **2016,** *8,* 2111-2119.

[16] J. Miao, H.B. Yang, S.Y. Khoo, B. Liu, *Nanoscale* **2013**. *5*, 11118-11124.

[17] M. Prasad, V. Sharma, R. Aher, A. Rokade, P. Ilaiyaraja, C. Sudakar, S. Jadkar, *J. Mater. Sci.* **2017**, *52*, 13572-13585.

Entry for the Table of Contents
FULL PAPER

Text for Table of Contents

*Author(s), Corresponding Author(s)**

Page No. Page No.

- Influence of Ag and Au over ZnO nanorods array is discussed in detail.
- Ag-Au embedded ZnO nanorods exhibit enhanced visible light absorption and PEC activity.
- ZnO nanorods loaded with Ag and Au on top surface exhibit remarkably enhanced PEC performance (~1.4 mA /cm^2 at a bias of 0.75 V).
- Ag-Au-ZNRs photo-anode exhibited effectual charge segregation and generation.